STING Deficiency Promotes Th17-Like Tfh to Aggravate the Experimental Autoimmune Uveitis

Zhuang Li,[1] Xiuxing Liu,[1] Zuoyi Li,[1] Zhiqiang Xiao,[1] Guanyu Chen,[1] Yangyang Li,[1] Jun Huang,[2] Yunwei Hu,[2] Haixiang Huang,[1] Wenjie Zhu,[1] Yuxun Shi,[1] Minzhen Wang,[1] Yanyan Xie,[1] Wenru Su,[1] Xiaoqing Chen,[1] and Dan Liang[1]

[1]State Key Laboratory of Ophthalmology, Zhongshan Ophthalmic Center, Sun Yat-Sen University, Guangdong Provincial Key Laboratory of Ophthalmology and Visual Science, Guangzhou, China
[2]Department of Ophthalmology, The Second Affiliated Hospital of Nanchang University, Nanchang, China

Correspondence: Dan Liang, State Key Laboratory of Ophthalmology, Zhongshan Ophthalmic Center, Sun Yat-Sen University, Guangdong Provincial Key Laboratory of Ophthalmology and Visual Science, 1/F, No. 7 Jinsui Rd., Zhujiang New Town, Tianhe District, Guangzhou 510060, China; liangdan@gzzoc.com.
Xiaoqing Chen, State Key Laboratory of Ophthalmology, Zhongshan Ophthalmic Center, Sun Yat-Sen University, Guangdong Provincial Key Laboratory of Ophthalmology and Visual Science, 1/F, No. 7 Jinsui Rd., Zhujiang New Town, Tianhe District, Guangzhou 510060, China; chenxiaoqing@gzzoc.com.

Zhuang Li, Xiuxing Liu, Zuoyi Li, Zhiqiang Xiao, Guanyu Chen, and Yangyang Li contributed equally to this study.

Received: July 4, 2024
Accepted: January 12, 2025
Published: March 5, 2025

Citation: Li Z, Liu X, Li Z, et al. STING deficiency promotes Th17-Like Tfh to aggravate the experimental autoimmune uveitis. *Invest Ophthalmol Vis Sci.* 2025;66(3):8. https://doi.org/10.1167/iovs.66.3.8

Purpose. The purpose of this study was to explore the underlying mechanism that Th17-like T follicular helper cells (Tfh) orchestrated by STING signaling have a pathogenic role in experimental autoimmune uveitis (EAU).

Methods. The differences of transcriptome and gene ontology (GO) pathway of Tfh between EAU and control mice were analyzed by single-cell RNA sequence (scRNA-seq) and bulk RNA sequence. Additionally, draining lymph nodes (DLNs) were extracted to verify the expression of IL-17A and IFN-γ in Tfh from EAU and control mice by flow cytometry. Then, the scRNA-seq and flow cytometry were used to explore the different proportion of Tfh between STING deficiency (*Sting*$^{-/-}$) mice and wild type (WT) mice. In vitro, naïve CD4$^+$ T cells were isolated from *Sting*$^{-/-}$ mice and WT mice to induce the Tfh under the induction condition. In addition, flow cytometry was used to detect the different induction ratio and the IL-17A expression between 2 groups of naïve CD4$^+$ T cells.

Results. Compared with control mice, marked increase of Tfh was observed in EAU, accompanied by elevated levels of Th1 and Th17 cells. Moreover, Th17-related genes, such as *Rorc*, *Il22*, *Il23r*, *Il17a*, and *Il17f*, and the corresponding GO pathways were upregulated in Tfh from EAU. The scRNA-seq showed that a higher proportion of Tfh was observed in the DLNs from *Sting*$^{-/-}$ mice than WT mice, which was verified by flow cytometry. When STING was knocked out, the Tfh was characterized with upregulated Th17-related phenotype in vivo, and there was a higher induction ratio of Tfh whose IL-17A expression was significantly increased in vitro. Notably, the STING expression of CD4$^+$ T cells was downregulated in the EAU. STING-deficient EAU mice displayed more severe retinal inflammation, characterized by massive infiltration of CD4$^+$ T cells, including Th1 and Th17 subsets. Importantly, treatment with a STING agonist alleviated inflammation of EAU.

Conclusions. Th17-like Tfh cells play a pathogenic role in the EAU. STING deficiency promotes the differentiation and phenotypic transformation of Th17-like Tfh cells, exacerbating the inflammatory response in EAU. These findings highlight the potential of targeting STING to modulate Tfh cells as a therapeutic strategy for uveitis.

Keywords: autoimmune uveitis, T follicular helper cells, Th17-like Tfh, stimulator of interferon genes

Autoimmune uveitis (AU) is a sight-threatening intraocular inflammatory disease. It is recognized that T helper (Th) cells play a predominant role in the development of ocular immunity.[1] Th cells are a group of highly heterogeneous CD4$^+$ T cells, among which T helper 1 (Th1) cells and T helper 17 (Th17) cells are the main pathogenic cells in AU, whereas regulatory T cells (Treg) are therapeutic.[2,3] T follicular helper (Tfh) cells constitute an important subgroup in Th, yet their precise role in AU remains unclear.

The Tfh cells are characterized with enriched surface molecules including CD4, programmed cell death protein 1 (PD-1), C-X-C motif chemokine receptor type 5 (CXCR5), intracellular cytokine interleukin-21 (IL-21) and endonuclear transcription factor B cell lymphoma 6 (BCL-6).[4–6] They mainly exist in the germinal centers (GCs) of lymphoid organs to promote follicular development and the reaction of GCs B cells.[4] Previous studies have demonstrated that Tfh cells contribute to autoimmune diseases by dysregulating autoantibodies and facilitating ectopic follicle formation, thereby influencing other pathogenic immune cells.[7,8] Recently, emerging evidence suggests that abnormal expansion and phenotypic transformation of Tfh cells into Th1-like, Th2-like, or Th17-like Tfh subsets are associated with human autoimmune diseases,[9,10] including rheumatoid

arthritis (RA) and systemic lupus erythematosus (SLE).[11–13] For example, Ma X et al. reported that Tfh-Th1 like cells (CD4$^+$, CXCR5$^+$, CXCR3$^+$, Bcl-6$^+$, T-bet$^+$, IL-21$^+$, and IFN-γ^+) were characteristically expanded in patients with SLE.[12] Similarly, Tfh cells expressing the IL-17A and IL-6, referred to as Th17-like Tfh cells, were elevated in patients with neuromyelitis optica spectrum disorder.[14] Despite these findings, the underlying mechanism that promotes the pathogenic phenotype of Tfh in autoimmune disease is ambiguous.

Stimulator of interferon (STING) is an innate immune adaptor which can detect pathologic DNA to modulate the immune homeostasis by type I IFN (IFN-α/β).[15,16] The STING signaling not only mediates protective immune defense against microbe infection but also supports the anti-tumor immunity to suppress the growth of the tumor.[17] However, aberrant STING expression has also been implicated in the pathogenesis of autoimmune and inflammatory disease, such as RA and multiple sclerosis (MS).[18,19] Besides, it has been reported that STING is involved in regulating the immune cell fate decision such as polarization, senescence, activation, and function.[20–22] For instance, Yang W et al. showed that stimulating STING could transform IFN-γ^+ Th1 cells into IL-10$^+$ IFN-γ^+ Th1 cells to alleviate colitis.[23] Recently, Barbet G et al. also revealed that IFN-β signaling could regulate the Tfh differentiation during Gram-negative bacterial infection.[24] These findings raise the question of whether STING might also affect the phenotype transformation of Tfh cells. Given the importance of Tfh cells in immune response, understanding the regulatory role of STING in Tfh cell biology could provide valuable insights into the development of targeted immunotherapies for autoimmune disorders.

In this study, we performed scRNA-seq and flow cytometry to explore the pathogenic phenotype transformation of Tfh cells in AU. Moreover, we sought to reveal the role of STING on Tfh differentiation and phenotype transformation in AU.

Methods

Mice

The 6 to 8 week old female C57BL/6J wild type (WT) mice and STING knockout (*Sting*$^{-/-}$) mice were purchased from Cyagen (Cyagen Biosciences [Suzhou] Inc., Jiangsu, China). These mice were maintained under specific pathogen-free conditions in Zhongshan Ophthalmic Center of Sun Yat-Sen University. In this study, all the animal experiments were carried out in accordance with the Institutional Animal Care and Use Committee of Zhongshan Ophthalmic Center of Sun Yat-Sen University, and were adhered to the Association for Research in Vision and Ophthalmology (ARVO) Statement for the Use of Animals in Ophthalmic and Vision Research.

Induction and Evaluation of Experimental Autoimmune Uveitis Mice Model

The experimental autoimmune uveitis (EAU) mice model (WT and *Sting*$^{-/-}$) was induced with 200 µg human interphotoreceptor retinoid-binding protein peptide 651-670 (hIRBP$_{651–670}$, LAQGAYRTAVDLESLASQLT, 2 mg/mL; Sangon Biotech, Shanghai, China) emulsified in the same volume of complete Freund's adjuvant (CFA) consisting of 2.5 mg/mL mycobacterium tuberculosis H37RA (MTX; BD Difco, San Jose, CA, USA) through subcutaneous injection in the back and in both thighs on day 0. Meanwhile, EAU mice were intraperitoneally injected with 0.25 µg Bordetella pertussis toxin (PTX, 50 µg/mL; List Biological Laboratories, Campbell, CA, USA) on day 0. Besides, the same dosages of PTX were injected intraperitoneally on day 2. EAU mice were administrated with STING agonist DMXAA (5 mg/kg/day) by intraperitoneal injection from day 3 to day 14. On day 14, EAU mice were anesthetized to examine the retina, and euthanized to evaluate pathological scores, as previously described.[3]

Induction of Tfh In Vitro

The CD44^{low} CD62L^{high} CD4$^+$ naïve T cells were sorted from lymph nodes and spleens of WT mice and *Sting*$^{-/-}$ mice by autoMACS Pro Separator (Miltenyi Biotec, Germany). Then, the purity of naïve CD4$^+$ T cells was examined with BD LSR Fortessa Flow Cytometer (BD Bioscience, San Jose, CA, USA). The naïve CD4$^+$ T cells (purity over 95%, 0.2 million/well) were seeded into 96-well-plate which had been coated by 10 µg/mL anti-CD3 (catalog #100239; Biolegend, San Diego, CA, USA). Then, naïve CD4$^+$ T cells were cultured with 10% fetal bovine serum (FBS) 1640 RPMI medium, which contained 2 µg/mL anti-CD28 (catalog #102115; Biolegend), 10 ng/mL IL-6 (catalog #406-ML-005/CF, R&D, USA), 5 µg/mL anti-IFN-γ (catalog #505833, Biolegend), 5 µg/mL anti-IL-4 (catalog #504121, Biolegend), 30 ng/mL IL-21 (catalog #210-21, PEPRO TECH, Thermo Fisher Scientific), and 10 ng/mL anti-TGFβ (catalog #BE0057; Bioxcell, USA) for 4 days before being analyzed, as previously described.[25,26] As for the negative control group (Th0), naïve CD4$^+$ T cells were only induced with 10 µg/mL anti-CD3 and 2 µg/mL anti-CD28 in 10% FBS 1640 RPMI medium for 4 days. Finally, we collected the induced cells to examine the induction ratio of Tfh (zombie$^-$ CD4$^+$ CXCR5$^+$ PD-1$^+$; and zombie$^-$ CD4$^+$ CXCR5$^+$ PD-1$^+$ IL-17A$^+$) in both the WT and the *Sting*$^{-/-}$ groups.

Flow Cytometry

First, Zombie NIR Fixable Viability Kit (catalog #423105; Biolegend) was applied to detect the cell activity. Then, the fluorochrome-conjugated antibodies for cell surface markers including CD45 (BV510, Clone 30-F11, catalog #103137), CD4 (PerCP-Cy5.5, Clone 1.5, catalog #100434), CD25 (PE-Cyanine7, Clone PC61, catalog #102016), CD44 (APC, Clone IM7, catalog #103011), CD62L (FITC, Clone MEL-14, catalog #104406), PD-1 (APC-Cyanine7, Clone 29F.1A12, catalog #135223 and #135209), CXCR5 (BV421, Clone L138D7, catalog #145511; APC, Clone L138D7, catalog #145505), and IL-23R(BV421, Clone 12B2B64, catalog #150907; all purchased from Biolegend) were stained according to the previously described method.[27] In addition, we also made isotype control for PD-1 (rat IgG2a, APC/Cyanine7 isotype control, catalog #135223 and #400511) and CXCR5 (rat IgG2b, Brilliant Violet 421 isotype control, catalog #400639; APC isotype control, catalog #400611). As for IL-23R staining, we made FMO control. The gating scheme and the gating controls are shown in Supplementary Figure S7.

For intracellular straining, cells were stimulated for 4 to 6 hours with Cell Activation Cocktail (with Brefeldin A; Biolegend, catalog #423303). Then, the cells were harvested, and stained with Zombie NIR Fixable Viability Kit and fluorochrome-conjugated antibodies for cell surface mark-

ers before fixation and permeabilization. Then, the intracellular cytokines including IFN-γ (BV785, Clone XMG1.2, catalog #505838) and IL-17A (BV650, Clone IM7, catalog #103011; both purchased from Biolegend), and the transcription factor Foxp3 (FITC, Clone FJK-16s, catalog #11-5773-82; eBioscience, Thermo Fisher Scientific, Waltham, MA, USA) were stained. Finally, the data were analyzed with FlowJo (TreeStar, Ashland, OR, USA).

Western Blotting

The single CD4$^+$ T cells were isolated from lymph nodes of EAU (WT mice, $n = 3$) and control mice (WT mice, $n = 3$) by flow cytometry, then they were extracted using the whole-cell lysis assay kit (KeyGen Biotech, Nanjing, China). The cell lysates were resuspended using an SDS-PAGE protocol and then transferred to nitrocellulose membranes (Both Bio-Rad, Hercules, CA, USA) as previously described. The membranes were immunoblotted with the following monoclonal antibodies (mAbs; Cell Signaling Technology [CST], Shanghai, China): anti-STING (catalog #13647) and anti-β-actin (catalog #8457S), which was blocked with 5% nonfat milk in TBS Tween for 2 hours at room temperature. Then, the membranes were immunoblotted with anti-rabbit IgG secondary antibody conjugated to horseradish (catalog #7074; CST). Finally, the membranes blots were visualized with SuperSignal West Atto Ultimate Sensitivity Substrate (Thermo Fisher Scientific; catalog #A38555), and the images were analyzed using ImageJ software (National Institutes of Health [NIH], Bethesda, MD, USA).

Single Cell RNA Sequencing

Preparation of Draining Lymph Nodes Cells for scRNA-Seq. The draining lymph nodes (DLNs) were extracted from control, EAU, WT, and *Sting*$^{-/-}$ mice, and prepared into DLNs cell suspensions by grinding and filtering through nylon mesh. The cells were then obtained by centrifugation at 1200 rpm for 5 minutes and used for subsequent studies after resuspension using 1640 medium (with 10% FBS). Finally, the cells from the same group of three mice were merged into a sequencing sample to ensure enough cells for scRNA-seq.

Data Alignment, Processing, and Aggregation. Chromium Single Cell 5′ Library (10X Genomics, Genomics chromium platform Illumina NovaSeq 6000), Chip Kit (10X Genomics), Gel Bead, and Multiplex Kit were used to transform the DLNs cell suspensions into barcoded scRNA-seq libraries. The CellRanger software, in which the count pipeline was used to demultiplex and barcode the sequences based on the mm10 (mouse) reference genome, was applied to preliminary process the sequencing data. FastQC software was used to check library quality after the initial processing of sequencing data by CellRanger software (version 4.0; 10X Genomics). The Seurat package (version 4.0.4) was used to exclude DLNs cells with <500 genes and >15% mitochondrial genes.[28] Finally, the cells were subsequently analyzed for normalization, dimension reduction, clustering, and differential expression genes (DEGs) analysis using the Seurat software package with the default parameters (like PCA, resolution parameters). The number of cells and genes per sample used for analysis are listed in Supplementary Table S1.

DEGs Analysis. Cell types with missing or fewer than three cells in the comparison group were filtered out prior to DEGs analysis. The DEGs analysis was performed for each cell type separately between groups using the "FindMarkers" function of the Seurat software package (version 4.0.4). DEGs between the EAU and control groups were first identified to generate a dataset of EAU-associated DEGs (EAU-DEGs) ($|\text{LogFC}| > 0.25$, $P < 0.05$). The DEGs between the control and *Sting*$^{-/-}$ groups were later identified to create a Sting-related DEGs dataset ($|\text{LogFC}| > 0.25$, $P < 0.05$).

Gene Ontology Enrichment Analysis. The Metascape web tool was used to perform the GO biological process and pathway analysis of the input DEGs. Among the first 30 enriched GO pathways, we visualized 10 pathways associated with the upregulated or downregulated DEGs using the "ggplot2" R package.

Pseudotime Trajectory Analysis. We used the Monocle 2 R package to analyze the developmental pseudotime of Tfh-related subsets and assess the impact of EAU or *Sting*$^{-/-}$ on their trajectory.[29,30] Following the Monocle vignette, the UMI count data served as the input, and DEGs identified among the subsets were selected to order the cells. The trajectory structure was visualized in two-dimensional space using the DDRTree dimensionality reduction algorithm, with cells ordered along pseudotime using default parameters. We then plotted DEGs associated with Tfh differentiation across the inferred developmental pseudotime, aligning cell subset and group annotations along the pseudotime axis based on bins.

Bulk RNA Sequencing

Total cells isolated from DLNs and the spleens of EAU mice and control mice were stained with Zombie dye and fluorochrome-conjugated antibodies including CD4, PD-1, and CXCR5. Then, the Tfh cells characterized with Zombie$^-$ CD4$^+$ CXCR5$^+$ PD1$^+$ were sorted (100% purity) by flow cytometry. Before lysed with TRIzol (Invitrogen), these isolated Tfh ($2*10^6$ cells) were washed twice with PBS. The total RNA was extracted with Direct-zol RNA MicroPrep kits (Zymo Research, R2062), according to the manufacturer's protocol. The total RNA was processed by the Yale Center for Genome Analysis using the Ribo-Zero rRNA Removal Kit, and the libraries were constructed and subjected to standard Illumina HiSeq2000 sequencing and obtained >40 million reads for each sample. The raw bulk RNA-seq reads were aligned to the mice reference genome GRCm39. The transcripts were analyzed by R (4.0.3). The R package limma was used to identify the DEGs between EAU mice and control mice with a fold change >2 and P value < 0.05.

Immunofluorescence

DLNs were extracted from the control, EAU, WT, and *Sting*$^{-/-}$ mice, and immediately immersed in 4% paraformaldehyde for fixation. The fixed DLNs tissues were dehydrated in a gradient sucrose solution (first in 10%, then in 20%, and last in 30%) for 6 hours in each of the steps, and embedded in optimal cutting temperature (OCT) compound and stored at −80°C. Frozen tissues with OCT were then sectioned into 10 µm-thick slices. The prepared sections were washed with phosphate-buffered saline (PBS) at room temperature and blocked with 3% bovine serum albumin (BSA) in PBS for 2 hours at room temperature. Primary antibodies (anti-PD-1, catalog #ab214421, Abcam; anti-CXCR5, catalog #MAB6198, R&D) diluted in blocking solution were applied, and the sections were incubated with mixed antibodies overnight

Investigative Ophthalmology & Visual Science

at 4°C in a humidified chamber. Subsequently, the sections were incubated with fluorophore-conjugated secondary antibodies and anti-CD4 antibody (conjugated FITC) (catalog #96127; CST) at room temperature for 2 hours in the dark. After washing, the sections were counterstained with DAPI and mounted with an anti-fade mounting medium. Images were captured using a Zeiss LSM 980 confocal laser scanning microscope.

Statistical Analysis

Data are presented as mean ± SD from three independent experiments. For comparisons between the two groups, the Student's unpaired *t*-test was utilized in flow cytometry, RT-qPCR, Western blot, and clinical and pathological scores. Additionally, for comparison of the genes' expression between the two groups in scRNA-seq, two-sided Wilcoxon test within the function "FindallMarkers" of the Seurat R package was used. For *P* value calculation in the GO biological process and pathway terms, hypergeometric test in Metascape webtool was adopted. Further statistical details of the experiments can be found in each figure legend. A statistically significant difference was considered when $^{*}P < 0.05$, $^{**}P < 0.01$, $^{***}P < 0.001$, and $^{****}P < 0.0001$, whereas ^{ns}P meant no significance. All the statistical analyses were conducted using GraphPad Prism version 10.

Results

Tfh Are Increased in EAU

We collected single cells from the DLNs of control mice and EAU mice to perform scRNA-seq at day 14 after immunization (schematic shown in Supplementary Fig. S1A).

We identified 10 major cell types: $CD4^+$ T cells (CD4), $CD8^+$ T cells (CD8), B cells (BC), T and B cells (TBC), proliferative T cells (Pro-T), natural killer cells (NK), conventional dendritic cells (cDCs), plasmacytoid dendritic cells (pDCs), monocytes (Mono), macrophages (Macro), and neutrophils (Neu) based on their corresponding marker genes (Fig. 1A, Supplementary Fig. S1B, Supplementary Table S2). To analyze $CD4^+$ T cell subsets in detail, $CD4^+$ T cells were first subdivided into $CD4^+$ naïve T cells (CD4NA) and $CD4^+$ memory T cells (CD4TM) by *Sell*, *Cd44*, and *Lef1*[31] (Figs. 1B, 1C, Supplementary Table S3). CD4TM was higher in EAU mice which was consistent with previous studies[31] (Fig. 1D). We separated $CD4^+$ TM into 5 subsets: *Foxp3*$^+$ *Il2ra*$^+$ Treg, *Ifng*$^+$ *Nkg7*$^+$ Th1, *Il17a*$^+$ *Cxcr6*$^+$ Th17, *Cd40lg*$^+$ *Cxcr5*$^+$ *Pdcd1*$^+$ *S1pr1*^{low} Tfh, and *Cd40lg*$^+$ *Cxcr5*$^{-/low}$ *Ccr7*$^+$ *S1pr1*$^+$ Tfh precursor (pre-Tfh) in both of the two groups (Fig. 1E, Supplementary Table S4). A previous study has reported that pre-Tfh requires further stimulation with antigen to transform into Tfh.[32] The individual t-SNE plots and violin plots about $CD4^+$ TM cells and Tfh for EAU and control group are shown in Supplementary Figure S1C to S1E. As known, T-helper (Th1 and Th17) cells were increased while the Treg were decreased in the EAU mice at day 14 after immunization. Notably, Tfh was increased in the EAU mice compared with the control mice (Fig. 1F). Furthermore, we also analyzed the transcription factors associated with Tfh including *Batf*, *Bcl6*, *c-Maf*, *Irf4*, and *Stat3* in the CD4TM from EAU and control group by DEGs and RT-qPCR. Compared with the control group, the expressions of *Batf*, *Bcl6*, *c-Maf*, and *Stat3* were increased in CD4TM from EAU mice, whereas the expression of *Irf4* was of no significant difference between the two groups which were verified by RT-qPCR (Supplementary Figs. S2A, S2B). These data show that T cells are endowed with the potential to transform into Tfh cells in EAU, rather than control mice.

We used the flow cytometry to verify the proportion of Th1, Th17, and Tfh in EAU and control mice, which was in consistence with scRNA-seq results (Figs. 1G–J, Supplementary Figs. S7A, S7B). Moreover, we conducted immunofluorescence and found that there were much more Tfh in DLNs of EAU than in the control mice (Supplementary Fig. S3A).

In sum, these data suggest that Tfh cells participate in inflammatory response in the EAU.

Tfh in EAU Are Characterized With Th17-Related Genes

To reveal the transcriptome difference, we further analyzed the Tfh between EAU mice and control mice by scRNA-seq. We used the volcano plot to show the DEGs of Tfh between EAU and control mice (Fig. 2A, Supplementary Table S5). We found that the genes associated with Th17 differentiation, such as *S100a8*, *S100a9*, *Fos*, and *Jund* were enriched in Tfh from EAU compared to Tfh from the control mice, which were separately shown with violin plots (Fig. 2B). In addition, Tfh in EAU were characterized with the Th17 related function pathway, such as IL-17 signaling pathway, positive regulation of inflammatory response, and regulation of type I interferon production (Fig. 2C). Additionally, pre-Tfh cells were characterized with higher expressions of Th17-related genes, such as *Fos*, *Jund*, *Hif1a*, *Pim1*, *Klf6*, *Bhlhe40*, and *Rora* in EAU (see Supplementary Fig. S2C). To further explore the pathogenic function of Tfh in EAU, we isolated Tfh ($CD4^+$ $CXCR5^+$ $PD\text{-}1^+$) from the DLNs in both the control mice and the EAU mice to perform the bulk RNA-seq. We conducted a DEGs analysis of Tfh between control mice and EAU. In EAU, Tfh exhibited upregulated Th17-related genes (*Rorc*, *Il22*, *Il23r*, *Il17a*, *Il17f*, and *Il1r1*), inflammation-related genes (*S100a9* and *S100a8*), and genes related to T cell migration (*Ccr1* and *Ccr2*; Figs. 2D, 2E, Supplementary Table S6). Compared with the control mice, the pathways related to Th17 differentiation and function, such as Th17 cell differentiation, IL-17 signaling pathway, JAK-STAT signaling pathway, and MAPK signaling pathway were enriched in the Tfh from EAU, which were accordant with scRNA-seq results (Fig. 2F).

To further investigate the fate differentiation of Tfh cells in EAU, we utilized the Monocle 2 R package to construct single-cell trajectories. CD4NA, pre-Tfh, and Tfh cells were mapped onto these trajectories based on their transcriptomic changes (Supplementary Fig. S2D). Our analysis revealed that the naïve subset was primarily located in early pseudotime, whereas the pre-Tfh and Tfh cells were predominantly found in later pseudotime. Notably, pre-Tfh cells emerged during the mid-phase and gradually decreased in the later phase (Supplementary Fig. S2E). We further examined the expression transitions of established marker genes associated with T cell differentiation along the pseudotime continuum. The results indicated a gradual decline in naïve markers, accompanied by a corresponding increase in Tfh markers (Supplementary Fig. S2F). These pseudotime reflects the progressive differentiation states of Tfh cells. Additionally, we observed that control cells were dominant in early pseudotime, whereas EAU cells were more preva-

Investigative Ophthalmology & Visual Science

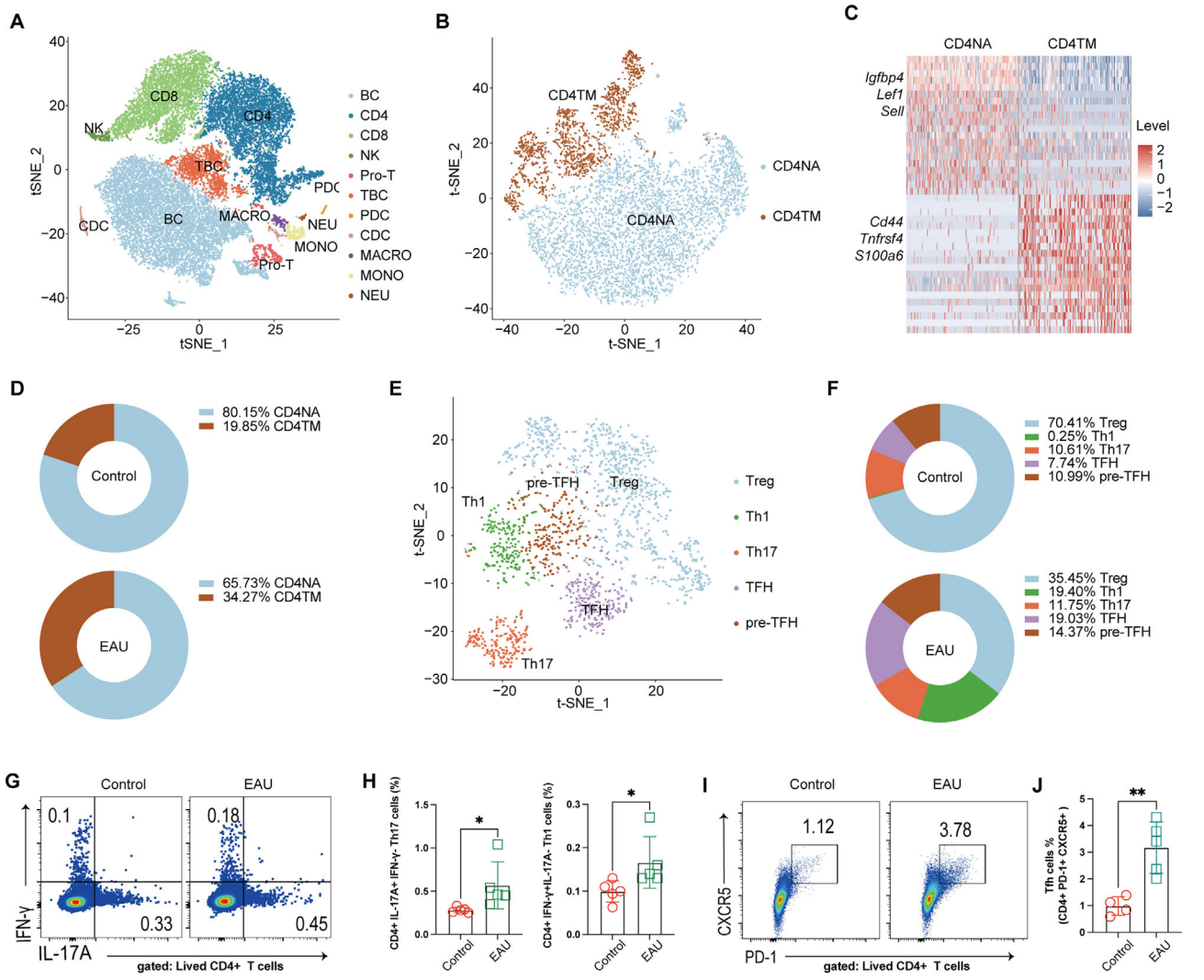

Figure 1. Tfh cells participate in inflammatory response in the EAU. (**A**) Distribution of lymphocyte subsets, including BC, CD4, CD8, NK, Pro-T, TBC, pDC, cDC, Mono, Macro, and Neu in DLNs of EAU and control mice, projected on a single t-SNE plot. (**B**, **C**) Distribution of segregated CD4$^+$ T cells subsets (CD4NA and CD4TM cells) projected on a single t-SNE plot; heat maps show scaled expression of discriminative genes for each cell type and subset with color scheme based on z-score distribution from −2 (*blue*) to 2 (*red*). (**D**) The pie chart showing the relative percentage of immune subpopulations (CD4NA and CD4TM cells) between the control (*top*) and the EAU (*bottom*) mice. (**E**) Distribution of segregated CD4TM subsets in DLNs of EAU and control mice, including Treg, Th1, Th17, Tfh, and pre-Tfh, projected on a single t-SNE plot. (**F**) The pie chart showing the relative percentage of immune subpopulations of CD4TM (Treg, Th1, Th17, Tfh, and pre-Tfh) between the control mice (*top*) and the EAU (*bottom*) mice. (**G**, **H**) The representative flow cytometry data and bar diagrams show proportions of Th1 and Th17 cells from DLNs in both control mice and the EAU mice. (**I**, **J**) The representative flow cytometry data and bar diagrams show the proportion of Tfh cells from DLNs in both the control mice and the EAU mice. Data presented as means ± standard deviations, with *$P < 0.05$, **$P < 0.01$, ***$P < 0.001$, and ****$P < 0.0001$. Data are representative of at least three independent experiments (except scRNA-seq).

lent in late pseudotime (Supplementary Fig. S2G). As Tfh markers increased, there was also a marked upregulation of Th17-related genes in late pseudotime (see Supplementary Fig. S2F), suggesting that EAU may induce Th17-like Tfh cells.

Next, we used the flow cytometry to verify the different phenotype of Tfh in DLNs between the control mice and the EAU mice. The Tfh from EAU could secrete much more IL-17A than IFN-γ (Figs. 2G, 2H). Additionally, IL-23R, a surface maker of pathogenic Th17, was upregulated in the Tfh of EAU (Figs. 2I, 2J, Supplementary Fig. S7C). We also verified that IL-17A were secreted by Th17-like Tfh rather than $\gamma\delta$ T cells (Supplementary Figs. S6A, S6B).

In sum, these results show that Th17-like Tfh cells play a pathogenic role in EAU.

STING Deficiency Promotes the Differentiation and Th17-Related Phenotype of Tfh

Because the GO pathway about regulation of type I interferon production was upregulated in the Tfh of EAU mice, we sought to investigate the impact of STING in Tfh. We collected single cells from the DLNs of *Sting*$^{-/-}$ and WT mice to perform scRNA-seq using the 10X Genomics library. According to canonical lineage markers, we subdivided

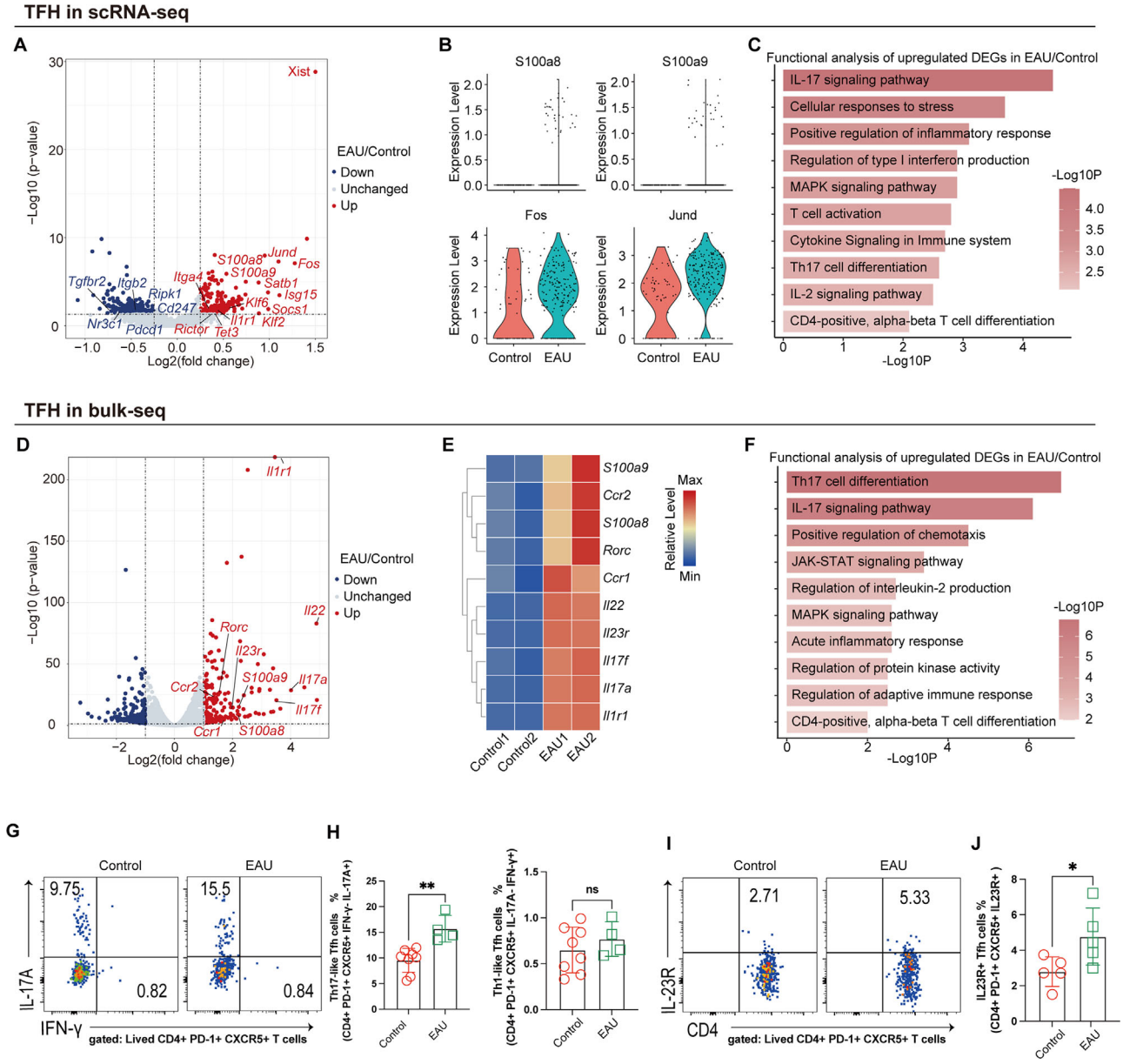

Figure 2. Tfh in EAU are characterized with Th17-related phenotype. (**A**) Volcano plot showing the upregulated and downregulated DEGs in Tfh between control and EAU groups by scRNA-seq. (**B**) The violin plot showing the expression of *S100a9*, *S100a8*, *Fos*, and *Jund* in Tfh between the control group and the EAU groups by scRNA-seq. (**C**) Representative functional analysis of upregulated DEGs in EAU/control comparisons by scRNA-seq. (**D**) Volcano plot showing the upregulated and downregulated DEGs in Tfh between control and EAU groups by bulk RNA-seq. (**E**) The heatmap showing the relative levels of marker genes in Tfh cells between control and EAU groups by bulk RNA-seq. Color scheme is based on z-score distribution from minimum (*blue*) to maximum (*red*). (**F**) Representative functional analysis of upregulated DEGs in EAU/control comparisons by bulk RNA-seq. (**G**, **H**) The representative flow cytometry data and bar diagrams show proportions of IL-17A$^+$ Tfh and IFN-γ^+ Tfh cells from DLNs in both the control mice and the EAU mice. (**I**, **J**) The representative flow cytometry data and bar diagrams show proportion of IL-23R$^+$ Tfh cells from DLNs in both control and EAU. Data presented as means ± standard deviations, with *$P < 0.05$, **$P < 0.01$, ***$P < 0.001$, and ****$P < 0.0001$. Data are representative of at least three independent experiments (except scRNA-seq and bulk RNA-seq).

CD4$^+$ effector T cells based on their main functions into T-helper (Th1 and Th17) cells, Treg cells, Tfh cells, and pre-Tfh cells by their key markers in both groups of mice (Figs. 3A, 3B). The proportion of Tfh, pre-Tfh, Th1, and Th17 all were higher in the *Sting*$^{-/-}$ mice, whereas the change in Tfh was the most significant (Fig. 3C). We also analyzed the transcription factors associated with Tfh including *Batf*, *Bcl6*, *c-Maf*, *Irf4*, and *Stat3* in the CD4TM from WT and *Sting*$^{-/-}$ mice by DEGs and RT-qPCR. Compared with the WT mice, the expressions of *Batf*, *Bcl6*, *c-Maf*, *Irf4*, and *Stat3* were increased in CD4TM from the *Sting*$^{-/-}$ mice, which were verified by RT-qPCR (Supplementary Figs. S4A, S4B). Then, we isolated the lymphocytes in DLNs from the *Sting*$^{-/-}$ mice and the WT mice to perform flow cytometry. We found STING deficiency promoted the proportion of Tfh in the DLNs (Figs. 3D, 3E). Moreover, immunofluorescence was conducted and showed that there were much more Tfh in DLNs of *Sting*$^{-/-}$ mice than WT mice, which was consis-

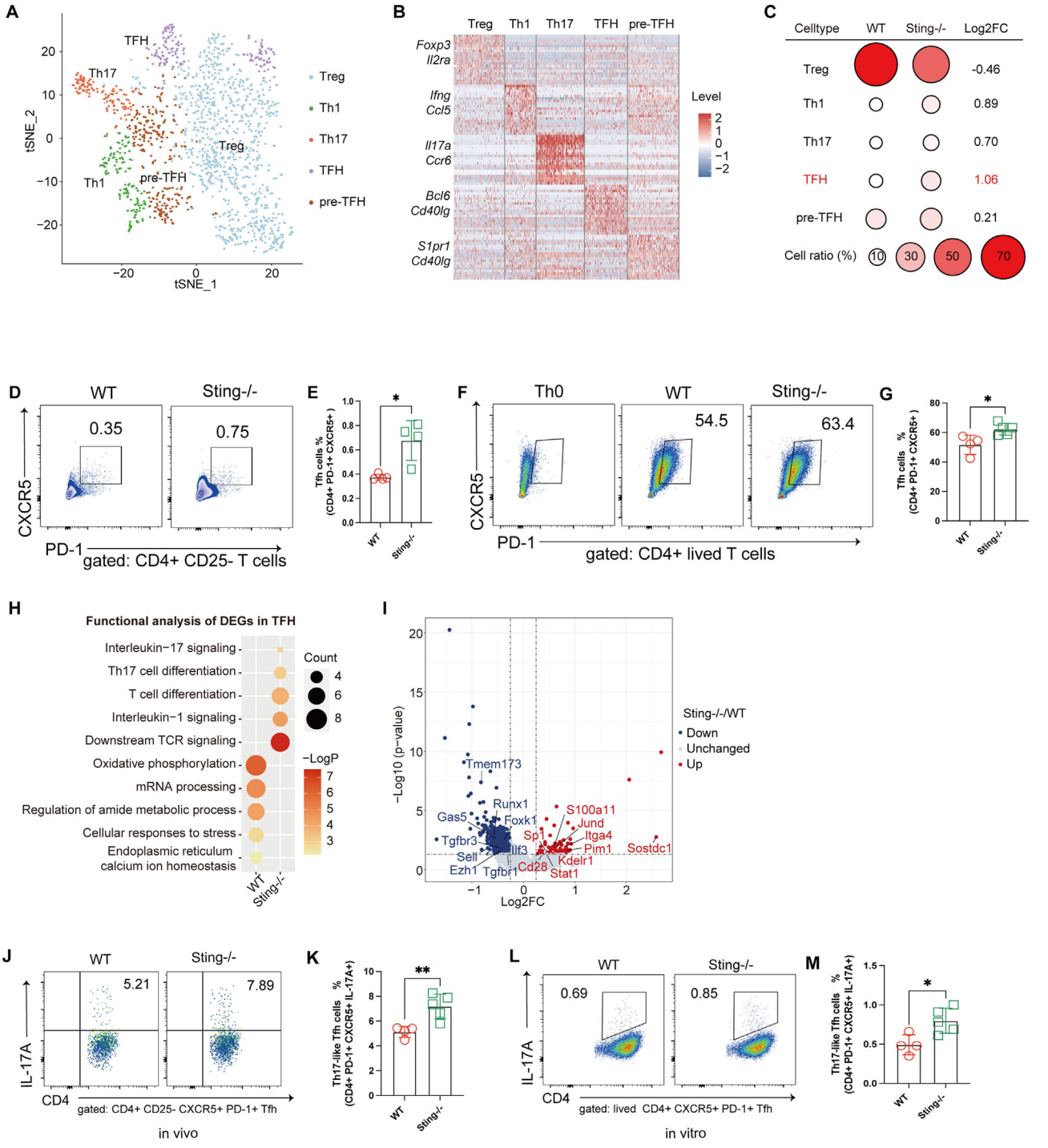

Figure 3. STING deficiency promotes the differentiation and Th17-related phenotype of Tfh. (**A**, **B**) Distribution of segregated CD4TM subsets in DLNs of WT and *Sting*$^{-/-}$ mice, including Treg, Th1, Th17, Tfh, and Pre-Tfh, projected on a single t-SNE plot. The heatmap showing the relative levels of marker genes in CD4TM subsets between the WT and *Sting*$^{-/-}$ mice groups by scRNA-seq. Color scheme is based on z-score distribution from minimum (*blue*) to maximum (*red*). (**C**) Dot plot showing the relative changes in cell ratios of CD4TM subsets (Treg, Th1, Th17, Tfh, and Pre-Tfh) between WT and *Sting*$^{-/-}$ mice groups. The numbers on the right indicate the Log2FC values of the cell ratios. (**D**, **E**) The representative flow cytometry data and bar diagrams show proportions of Tfh cells from DLNs in both WT and *Sting*$^{-/-}$ mice in vivo. (**F**, **G**) The representative flow cytometry data and bar diagrams show proportions of induced Tfh cells by CD4^{+} naïve T cells from both the WT mice and the *Sting*$^{-/-}$ mice in vitro. (**H**) A representative GO term and pathway analysis in Tfh cells of the WT mice and the *Sting*$^{-/-}$ mice. (**I**) Volcano plot showing the upregulated and downregulated DEGs in Tfh between WT and *Sting*$^{-/-}$ mice by scRNA-seq. (**J**, **K**) The representative flow cytometry data and bar diagrams show proportions of IL-17A^{+} Tfh cells (Th17-like Tfh) from DLNs in both the WT mice and the *Sting*$^{-/-}$ mice in vivo. (**L**, **M**) The representative flow cytometry data and bar diagrams show proportions of IL-17A^{+} induced Tfh cells (Th17-like Tfh) by CD4^{+} naïve T cells from both the WT mice and the *Sting*$^{-/-}$ mice in vitro. Data presented as means ± standard deviations, with **P* < 0.05, ***P* < 0.01, ****P* < 0.001, and *****P* < 0.0001. Data are representative of at least three independent experiments (except scRNA-seq).

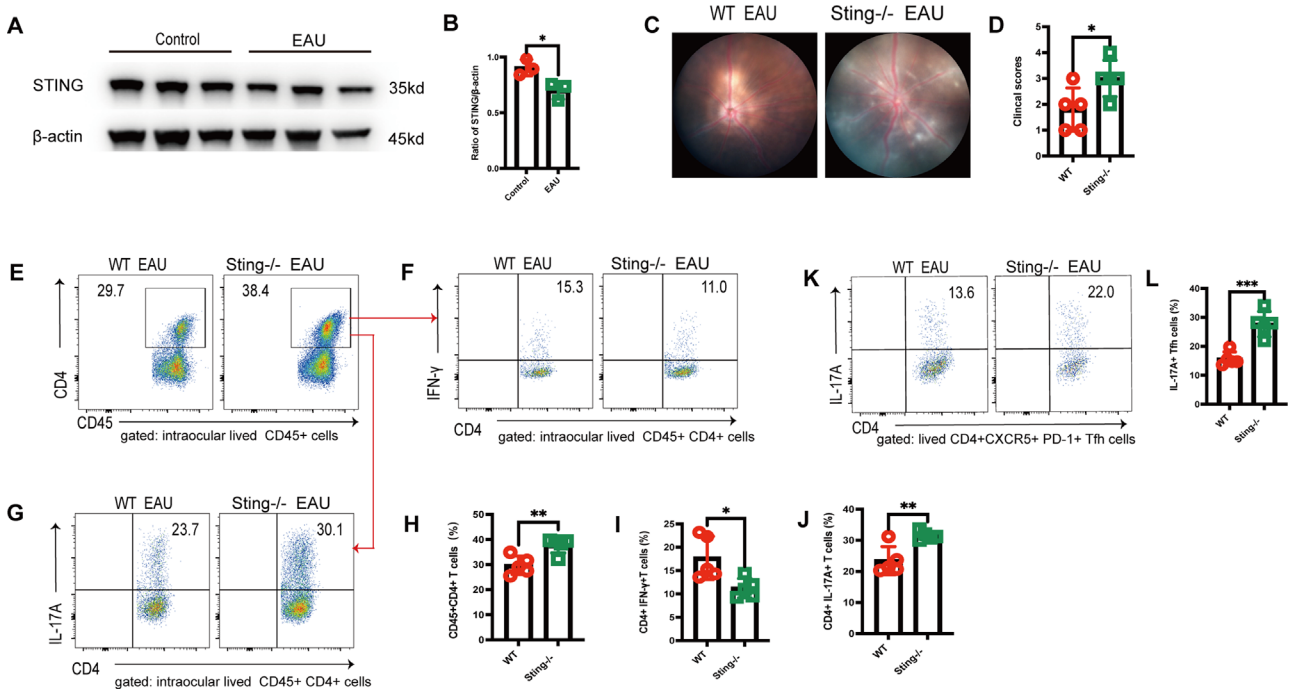

Figure 4. STING deficiency could facilitate the inflammation of EAU. (**A**, **B**) Immunoblots and histogram of expression of STING in CD4$^+$ T cells isolated from DLNs of control and EAU mice, with β-actin used as loading control. (**C**) Photographic images of ocular fundus of WT EAU and *Sting*$^{-/-}$ EAU showing retinal inflammation, with areas of inflammatory exudate and hemangiectasis. (**D**) Bar diagrams showing comparison of clinical inflammation scores in the WT mice and the *Sting*$^{-/-}$ EAU mice, with scores ranging from 0 (no disease) to 4 (maximal disease). (**E–J**) The representative flow cytometry data and bar diagrams show proportions of CD4$^+$ T cells, IFN-γ^+ CD4$^+$ T cells (Th1) and IL-17A$^+$ CD4$^+$ T cells (Th17) cells from eyes of the WT mice and the *Sting*$^{-/-}$ EAU mice. (**K**, **L**) The representative flow cytometry data and bar diagrams show proportions of IL-17A$^+$ Tfh cells (Th17-like Tfh) cells from DLNs of the WT mice and the *Sting*$^{-/-}$ EAU mice. Data presented as means ± standard deviations, with *$P < 0.05$, **$P < 0.01$, ***$P < 0.001$, and ****$P < 0.0001$. Data are representative of at least three independent experiments.

tent with flow cytometry results (Supplementary Fig. S5A). To investigate the differentiation ability to Tfh in vitro, we isolated naïve CD4$^+$ T cells from two groups to induce the Tfh. Compared with naïve CD4$^+$ T cells from WT mice, naïve CD4$^+$ T cells from *Sting*$^{-/-}$ mice had more potential to differentiate into Tfh (Figs. 3F, 3G). These results show that STING deficiency facilitates the Tfh polarization both in vivo and in vitro.

Then, we analyzed the DEGs in Tfh between STING deficiency and WT. The bubble diagram showed that the genes and signaling pathways associated with Th17 cell differentiation, IL-17 signaling pathway, IL-1 signaling pathway, and T cell differentiation were enriched in the *Sting*$^{-/-}$ Tfh, whereas the oxidative phosphorylation and regulation of amide metabolic process were downregulated (Figs. 3H, 3I, see Supplementary Table S7). To further describe the fate development of Th17-like Tfh between STING deficiency and WT, we also construct single-cell trajectories in which CD4NA, pre-Tfh, and Tfh cells were mapped based on their transcriptomic changes (see Supplementary Fig. S4C). Compared with the naïve CD4$^+$ T cells subset, Tfh cells were predominantly found in later pseudotime (see Supplementary Fig. S4D). Similarly, the expression transitions of genes associated with T cell differentiation showed a gradual decline in naïve markers, accompanied by a corresponding increase in Tfh and Th17-related markers along with time (see Supplementary Fig. S4E). WT cells were gradually decreased, whereas *Sting*$^{-/-}$ cells were gradually increased along the pseudotime (Supplementary Fig. S4F).

Moreover, we isolated immune cells in DLNs from WT and *Sting*$^{-/-}$ mice to compare the changes in the proportion of Th17-like Tfh cells between the two groups, and found that *Sting*$^{-/-}$ Tfh could secrete much more IL-17A (Figs. 3J, 3K). Additionally, we determined that IL-17A were secreted by Th17-like Tfh rather than $\gamma\delta$ T cells (Supplementary Fig. S6C). Furthermore, we isolated naïve CD4$^+$ T cells from *Sting*$^{-/-}$ mice and WT mice to induce the Tfh in vitro. Meaningfully, induced Tfh from *Sting*$^{-/-}$ naïve CD4$^+$ T cells had more potential to secrete the IL-17A (Figs. 3L, 3M). These results show that STING deficiency facilitates the Th17-like Tfh polarization both in vivo and in vitro.

In sum, these results suggest that STING deficiency orchestrates the Tfh to characterize the Th17-related phenotype.

STING Deficiency Could Facilitate the Inflammation of EAU

To verify whether STING could mediate autoimmune disease through Tfh cells in vivo, we first isolated CD4$^+$ T cells in DLNs from WT and EAU mice to conduct the Western blot, and found the STING expression was decreased in the CD4$^+$ T cells from EAU compared with the control mice (Figs. 4A, 4B). These data suggested that STING expression of CD4$^+$ T cells was impaired in EAU. Then, *Sting*$^{-/-}$ mice and WT mice were immunized with hIRBP$_{651\text{-}670}$ to induce EAU, and the mice were evaluated after 2 weeks. Compared to the WT EAU mice, the *Sting*$^{-/-}$ EAU mice had more

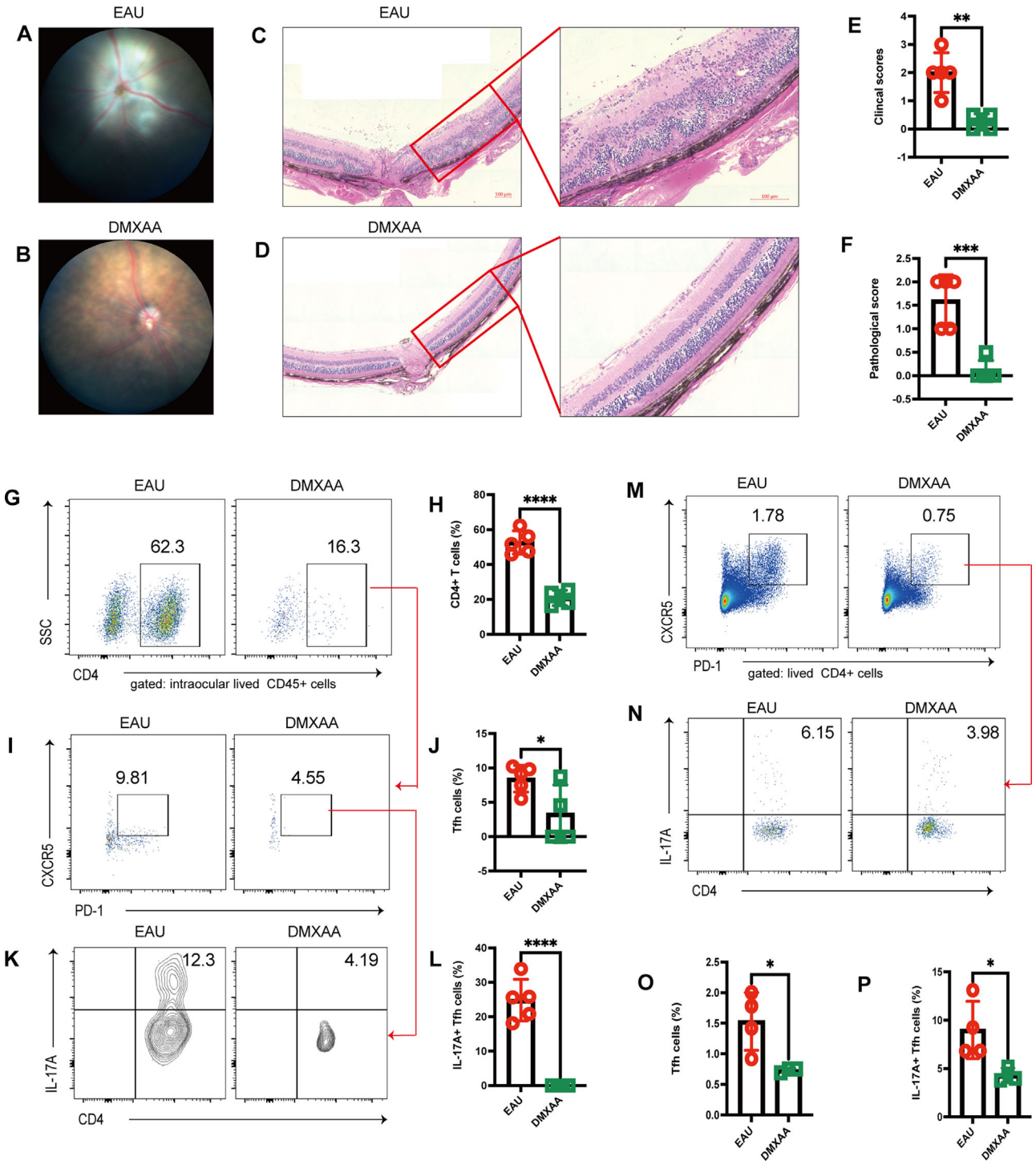

Figure 5. STING activation could alleviate EAU. (A, B) Photographic images of ocular fundus of EAU without treatment and DMXAA EAU showing retinal inflammation, with areas of inflammatory exudate and hemangiectasis. **(C, D)** Photomicrographs of H&E-stained tissue show pathological changes in retinas of EAU without treatment and DMXAA EAU mice, with areas of retinal detachment and lymphocytes infiltrates (scale bar = 100 µm). **(E)** Bar diagrams showing comparison of clinical inflammation scores in EAU without treatment and DMXAA EAU mice, with scores ranging from 0 (no disease) to 4 (maximal disease). **(F)** Histogram shows comparison of pathological disease severity scores ranging from 0 (no disease) to 4 (maximal disease). **(G–L)** The representative flow cytometry data and bar diagrams show proportions of $CD4^+$ T cells, Tfh, and IL-$17A^+$ Tfh cells (Th17-like Tfh, there was fewer $IL17^+$ Tfh cell points which resulted in the inability to be displayed in the contour plot) from eye of EAU without treatment and DMXAA EAU mice. **(M–P)** The representative flow cytometry data and bar diagrams show proportions of Tfh and IL-$17A^+$ Tfh cells (Th17-like Tfh) cells from DLNs of EAU without treatment and DMXAA EAU mice. Data presented as means ± standard deviations, with $^*P < 0.05$, $^{**}P < 0.01$, $^{***}P < 0.001$, and $^{****}P < 0.0001$. Data are representative of at least three independent experiments.

Investigative Ophthalmology & Visual Science

severe ocular inflammation, which was characterized by papilledema, vascular white sheath, and retinal detachment, as shown in the fundus pictures (Figs. 4C, 4D). The intraocular infiltrated CD4$^+$ T cells and Th17 were increased in the *Sting*$^{-/-}$ EAU mice, whereas the Th1 cells were decreased in the *Sting*$^{-/-}$ EAU mice consistently (Figs. 4E–J). These data verified that STING deficiency could facilitate the intraocular inflammation of EAU. In addition, we also detected the Th17-like Tfh in DLNs between WT EAU and *Sting*$^{-/-}$ EAU mice, and found that the Tfh from *Sting*$^{-/-}$ EAU mice had more potential to secrete IL-17A which further indicated that STING deficiency could promote the Th17-like Tfh to participate in the immune response in EAU (Figs. 4K, 4L).

Together, our data demonstrated that STING deficiency could facilitate the inflammation in both the retina and DLNs of EAU.

STING Activation Could Alleviate EAU

Because STING deficiency could promote the inflammation in EAU, we further investigated whether stimulating STING could treat EAU. We administrated EAU mice with STING agonist DMXAA (schematic shown in Supplementary Fig. S1A). Compared to EAU without treatment, we found that DMXAA could significantly alleviate retina inflammation characterized with less papilledema, and vascular white sheath in the fundus (Figs. 5A, 5B). The clinical scores were lower in the DMXAA group (Fig. 5E). Compared with the EAU mice, there were milder pathological change such as retinal detachment, lymphocyte infiltrates, and chorioretinal lesions in the DMXAA group shown in the hematoxylin and eosin (H&E; Figs. 5C, 5D) stain. The pathological scores were also lower in the DMXAA group than the EAU mice (Fig. 5F). Importantly, stimulating STING could also suppress the Tfh cells and Th17-like Tfh in retina (Figs. 5G–L, Supplementary Fig. S7D). These data showed that STING agonist could alleviate the damage and inflammation response of retina in EAU.

Additionally, we also investigated whether stimulating STING could suppress the Tfh in DLNs of EAU. We conducted the flow cytometry, and found that administrating DMXAA could significantly decrease Tfh and Th17-like Tfh compared with EAU mice without treatment (Figs. 5M–P, Supplementary Fig. S7E). These data revealed that stimulating STING could alleviate the inflammation of EAU by suppressing the differentiation of Th17-like Tfh.

In sum, these results suggest that targeting STING could be a novel method for uveitis therapy.

Discussion

In this study, we demonstrated that Tfh played a pathogenic role in uveitis through transforming into Th17-related phenotype, which was mediated by STING deficiency. Meaningfully, these findings established STING as a potential regulator in the differentiation and transformation of Th17-like Tfh, providing new insights into its role in autoimmune uveitis.

We utilized EAU, an established animal model,[1] to elucidate human uveitis pathogenesis. By performing scRNA-seq analysis of EAU, we observed significant increases in Th1, Th17, and Tfh cells, which underscored potential importance of Tfh in disease progression. Although Th1 and Th17 are recognized as crucial pathogenic cells in autoimmune uveitis,[1,2] the role of Tfh, a relatively newly identified subset of CD4$^+$ T cells, has not previously been widely studied in uveitis. Consistent with our findings, previous studies have implicated that the abnormal or excessive activation of Tfh cells contribute to autoimmune diseases development, such as MS,[33] psoriasis,[34] and SLE.[35] To conclude, our study suggests that Tfh cells contribute to the pathogenic progress of uveitis.

It has been reported that Tfh cells could be divided into heterogeneous subgroups, including Th1-like, Th2-like, and Th17-like Tfh depending on the co-expression of BCL6 and other lineage-determining transcription factors like T-bet, Gata3, or RORγt, respectively.[36–39] Due to the different transcription factors and cytokines, these Tfh subsets could play different roles in disease.[10,40] For instance, Th17-like Tfh are predominant in SLE and drive the promotion of disease,[12] whereas Th2-like Tfh are responsible for inducing functional antibody production during plasmodium falciparum infection.[41] The excess secretion of IFN-γ, IL-4, and IL-17A by Tfh subsets could amplify immune responses and promote disease.[37,42,43] Moreover, whereas Th17-like and Th2-like Tfh cells can stimulate B cells to produce antibodies, Th1-like Tfh cells lack this capability.[44] Thus, the heterogeneous subsets of Tfh cells play diverse roles in the development and progression of diseases. A deeper understanding of these Tfh subsets could facilitate the development of new therapeutic strategies, particularly in the fields of autoimmune diseases. However, it has not been revealed whether Tfh could differentiate into heterogeneous subsets in uveitis. The pathogenic function of Th17 cells and IL-17-producing T cells (e.g. $\gamma\delta$ T cells) in AU has been reported.[3,45] As known, pathogenic Th17 cells secrete pro-inflammatory cytokines, such as IL-17A and GM-CSF to facilitate the immune response and retina impairment.[46] Then, we dug deeper to investigate the characteristics of Tfh, and explored whether Tfh were equipped with Th17 phenotype and function in EAU. Interestingly, we observed increased Th17-like Tfh in EAU mouse models. Our study first revealed that the molecular (e.g. IL-23R and IL-17A) and pathways related to Th17 differentiation and function (e.g. IL-17 signaling pathway, JAK-STAT signaling pathway, and MAPK signaling pathway) were enriched in the Tfh from EAU. As known, the inflammatory factors, such as IL-23 and IL-6, could upregulate the PI3K-AKT, MAPK, and JAK-STAT3 signaling to promote the IL-17A secretion.[47,48] These results highlight that Tfh in EAU possess characteristics and function of Th17 cells, and amplify inflammatory responses, thereby driving disease progression.

As known, BCL-6 plays a crucial role in the Tfh development and differentiation.[49] Emerging evidence suggests that type I IFN signaling promotes humoral immunity in viral vector vaccination, including B cells and Tfh responses.[50] Besides, it has been reported that Gram-negative bacteria heightened Tfh differentiation via IFN-β-dependent secretion of IL-1β.[24] Recent studies have verified that STING, a facilitator of immune signaling that promotes cellular activation and type I interferon (IFN-α/β) production,[15,16] plays a pivotal role in immune cell function and differentiation.[20,21] For instance, STING activation in CD4$^+$ T cells could trigger Treg differentiation.[51] These previous studies have implied that STING would be a potential regulator in CD4$^+$ T cells differentiation. However, it is unclear whether STING signaling is involved in the fate and development of Tfh. In our study, we used the *Sting*$^{-/-}$ mouse for scRNA-seq and found Tfh cells were increased in *Sting*$^{-/-}$ mice, suggesting that

Investigative Ophthalmology & Visual Science

STING negatively regulates Tfh cells. Furthermore, we tried to figure out whether STING could also regulate Tfh differentiation. We explored further and found out that the differentiation of Tfh was facilitated by STING deficiency and *Sting*$^{-/-}$ Tfh could secrete much more IL-17A, which is aligned with research about STING in Th17 cells reported by Damasceno L et al.[22] Thus, these results suggest that STING deficiency promotes the transformation of Tfh cells into a Th17-like phenotype.

Moreover, we investigated the role of STING on Tfh cells by establishing an EAU model. We first found that the STING expression was lower in CD4^{+} T cells of EAU mice. In *Sting*$^{-/-}$ EAU mice, disease severity and the infiltration of Th17-like Tfh and Th17 cells were found to be elevated, confirming the influence of STING on Tfh cells. Meaningfully, stimulating STING could suppress Th17-like Tfh and alleviate inflammation in EAU. Consequently, these findings suggest that STING exerts a protective role by limiting the pathogenic transformation of Tfh cells in EAU.

However, it is important to acknowledge some limitations of our study. Although our in vitro and in vivo experiments provide strong evidence for the role of STING in Th17-like Tfh cell differentiation, future studies are warranted to elucidate the precise molecular mechanisms by which STING regulates the transformation of Tfh cells into a Th17-like phenotype.

In summary, our study demonstrates that Tfh cells contribute to the progression of EAU by exhibiting a Th17-like phenotype. STING acts as a negative regulator of Th17-like Tfh cell differentiation and function, highlighting its therapeutic potential in uveitis.

Acknowledgments

Supported by the China Postdoctoral Science Foundation (No. 2022M723624), the GuangDong Basic and Applied Basic Research Foundation (No. 2023A1515110965), and the National Natural Science Foundation of China (No. U22A20308).

Author Contributions: Z.L., X.L., Z.L., Z.X., G.C., and Y.L. designed the study, created the model, analyzed the data, and wrote the manuscript. W.Z., J.H., Y.H., and H.H. assisted in writing the manuscript. Y.S., M.W., and Y.X. provided guidance with the individual experiments and supervised the study. W.S. helped with the revision of the manuscript. X.C. and D.L. were responsible for the conception and design, revision of the manuscript, and approval of the final manuscript. All authors read and approved the final manuscript, and approved the version submitted for publication. All data needed to evaluate the conclusions in the paper are present in the paper and/or the Supplementary Materials.

Data Availability: The scRNA-seq data is deposited in the Genome Sequence Archive in BIG Data Center, Beijing Institute of Genomics (BIG, https://bigd.big.ac.cn/gsa/), Chinese Academy of Sciences. The data of WT and *Sting*$^{-/-}$ mice was deposited under the GSA Accession No. CRA006059. The data of control and EAU mice was under the GSA Accession No. CRA004687. The data analysis pipeline used in scRNA-Seq follows the description on the 10X Genomics and Seurat official websites. The analysis steps, functions, and parameters used are described in detail in the Materials and Methods section.

Disclosure: **Z. Li**, None; **X. Liu**, None; **Z. Li**, None; **Z. Xiao**, None; **G. Chen**, None; **Y. Li**, None; **J. Huang**, None; **Y. Hu**, None; **H. Huang**, None; **W. Zhu**, None; **Y. Shi**, None; **M. Wang**, None; **Y. Xie**, None; **W. Su**, None; **X. Chen**, None; **D. Liang**, None

References

1. Huang J, Li Z, Hu Y, et al. Azithromycin modulates Teff/Treg balance in retinal inflammation via the mTOR signaling pathway. *Biochem Pharmacol*. 2021;193:114793.
2. Wang C, Zhou W, Su G, Hu J, Yang P. Progranulin suppressed autoimmune uveitis and autoimmune neuroinflammation by inhibiting Th1/Th17 cells and promoting Treg cells and M2 macrophages. *Neurol Neuroimmunol Neuroinflamm*. 2022;9(2):e1133.
3. Li Z, Chen X, Chen Y, et al. Teriflunomide suppresses T helper cells and dendritic cells to alleviate experimental autoimmune uveitis. *Biochem Pharmacol*. 2019;170:113645.
4. Yu D, Walker LSK, Liu Z, Linterman MA, Li Z. Targeting TFH cells in human diseases and vaccination: rationale and practice. *Nat Immunol*. 2022;23(8):1157–1168.
5. Shao F, Zheng P, Yu D, Zhou Z, Jia L. Follicular helper T cells in type 1 diabetes. *FASEB J*. 2020;34(1):30–40.
6. Crotty S. T follicular helper cell biology: a decade of discovery and diseases. *Immunity*. 2019;50(5):1132–1148.
7. Craft JE. Follicular helper T cells in immunity and systemic autoimmunity. *Nat Rev Rheumatol*. 2012;8(6):337–347.
8. Crotty S. T follicular helper cell differentiation, function, and roles in disease. *Immunity*. 2014;41(4):529–542.
9. Gao X, Luo K, Wang D, et al. T follicular helper 17 (Tfh17) cells are superior for immunological memory maintenance. *Elife*. 2023;12:e82217.
10. Noto A, Suffiotti M, et al. The deficiency in Th2-like Tfh cells affects the maturation and quality of HIV-specific B cell response in viremic infection. *Front Immunol*. 2022;13:960120.
11. Mao M, Xu S, Lin L, et al. Impact of corticosteroids on the proportions of circulating Tfh cell subsets in patients with systemic lupus erythematous. *Front Med (Lausanne)*. 2022;9:949334.
12. Ma X, Nakayamada S, Kubo S, et al. Expansion of T follicular helper-T helper 1 like cells through epigenetic regulation by signal transducer and activator of transcription factors. *Ann Rheum Dis*. 2018;77(9):1354–1361.
13. Kim V, Lee K, Tian H, Jang SH, Diamond B, Kim SJ. IL-17-producing follicular Th cells enhance plasma cell differentiation in lupus-prone mice. *JCI Insight*. 2022;7(11):e157332.
14. Monteiro C, Fernandes G, Kasahara TM, et al. The expansion of circulating IL-6 and IL-17-secreting follicular helper T cells is associated with neurological disabilities in neuromyelitis optica spectrum disorders. *J Neuroimmunol*. 2019;330:12–18.
15. Woo SR, Fuertes MB, Corrales L, et al. STING-dependent cytosolic DNA sensing mediates innate immune recognition of immunogenic tumors. *Immunity*. 2014;41(5):830–842.
16. Webb LG, Veloz J, Pintado-Silva J, et al. Chikungunya virus antagonizes cGAS-STING mediated type-I interferon responses by degrading cGAS. *PLoS Pathog*. 2020;16(10):e1008999.
17. Guo Y, Jiang F, Kong L, et al. OTUD5 promotes innate antiviral and antitumor immunity through deubiquitinating and stabilizing STING. *Cell Mol Immunol*. 2021;18(8):1945–1955.
18. Willemsen J, Neuhoff MT, Hoyler T, et al. TNF leads to mtDNA release and cGAS/STING-dependent interferon responses that support inflammatory arthritis. *Cell Rep*. 2021;37(6):109977.
19. Woo MS, Mayer C, Binkle-Ladisch L, et al. STING orchestrates the neuronal inflammatory stress response in multiple sclerosis. *Cell*. 2024;187(15):4043–4060.e30.
20. Pan Y, You Y, Sun L, et al. The STING antagonist H-151 ameliorates psoriasis via suppression of STING/NF-κB-mediated inflammation. *Br J Pharmacol*. 2021;178(24):4907–4922.

21. Hou Y, Wei Y, Lautrup S, et al. NAD+ supplementation reduces neuroinflammation and cell senescence in a transgenic mouse model of Alzheimer's disease via cGAS-STING. *Proc Natl Acad Sci USA*. 2021;118(37):e2011226118.
22. Damasceno LEA, Cebinelli GCM, Fernandes MF, et al. STING is an intrinsic checkpoint inhibitor that restrains the TH17 cell pathogenic program. *Cell Rep*. 2022;39(8):110838.
23. Yang W, Yu T, Zhou G, et al. Intrinsic STING switches off pathogenetic programs of Th1 cells to inhibit colitis. *Cell Mol Gastroenterol Hepatol*. 2023;15(5):1161–1179.
24. Barbet G, Sander LE, Geswell M, et al. Sensing microbial viability through bacterial RNA augments T follicular helper cell and antibody responses. *Immunity*. 2018;48(3):584–598.e5.
25. Zhu F, McMonigle RJ, Schroeder AR, et al. Spatiotemporal resolution of germinal center Tfh cell differentiation and divergence from central memory CD4+ T cell fate. *Nat Commun*. 2023;14(1):3611.
26. Wan S, Ni L, Zhao X, et al. Costimulation molecules differentially regulate the ERK-Zfp831 axis to shape T follicular helper cell differentiation. *Immunity*. 2021;54(12):2740–2755.e6.
27. Huang J, Li Z, Hu Y, et al. Melatonin, an endogenous hormone, modulates Th17 cells via the reactive-oxygen species/TXNIP/HIF-1α axis to alleviate autoimmune uveitis. *J Neuroinflammation*. 2022;19(1):124.
28. Satija R, Farrell JA, Gennert D, Schier AF, Regev A. Spatial reconstruction of single-cell gene expression data. *Nat Biotechnol*. 2015;33(5):495–502.
29. Lv J, Zhang C, Liu X, et al. An aging-related immune landscape in the hematopoietic immune system. *Immun Ageing*. 2024;21(1):3.
30. Qiu X, Mao Q, Tang Y, et al. Reversed graph embedding resolves complex single-cell trajectories. *Nat Methods*. 2017;14(10):979–982.
31. Liu X, Su Y, Huang Z, et al. Sleep loss potentiates Th17-cell pathogenicity and promotes autoimmune uveitis. *Clin Transl Med*. 2023;13(5):e1250.
32. Vinuesa CG, Linterman MA, Yu D, MacLennan ICM. Follicular helper T cells. *Annu Rev Immunol*. 2016;34:335–368.
33. Schafflick D, Xu CA, Hartlehnert M, et al. Integrated single cell analysis of blood and cerebrospinal fluid leukocytes in multiple sclerosis. *Nat Commun*. 2020;11(1):247.
34. Niu J, Song Z, Yang X, Zhai Z, Zhong H, Hao F. Increased circulating follicular helper T cells and activated B cells correlate with disease severity in patients with psoriasis. *J Eur Acad Dermatol Venereol*. 2015;29(9):1791–1796.
35. Zhao Z, Xu B, Wang S, et al. Tfh cells with NLRP3 inflammasome activation are essential for high-affinity antibody generation, germinal centre formation and autoimmunity. *Ann Rheum Dis*. 2022;81(7):1006–1012.
36. Kaech SM. T-bet in Tfh cells: now you see me, now you don't. *J Exp Med*. 2018;215(11):2697–2698.
37. Fang D, Cui K, Mao K, et al. Transient T-bet expression functionally specifies a distinct T follicular helper subset. *J Exp Med*. 2018;215(11):2705–2714.
38. Hercor M, Anciaux M, Denanglaire S, Debuisson D, Leo O, Andris F. Antigen-presenting cell-derived IL-6 restricts the expression of GATA3 and IL-4 by follicular helper T cells. *J Leukoc Biol*. 2017;101(1):5–14.
39. Wu HY, Quintana FJ, Weiner HL. Nasal anti-CD3 antibody ameliorates lupus by inducing an IL-10-secreting CD4+ CD25− LAP+ regulatory T cell and is associated with down-regulation of IL-17+ CD4+ ICOS+ CXCR5+ follicular helper T cells. *J Immunol*. 2008;181(9):6038–6050.
40. Gao X, Luo K, Wang D, et al. T follicular helper 17 (Tfh17) cells are superior for immunological memory maintenance. *Elife*. 2023;12:e82217.
41. Chan JA, Loughland JR, de Labastida Rivera F, et al. Th2-like T follicular helper cells promote functional antibody production during Plasmodium falciparum infection. *Cell Rep Med*. 2020;1(9):100157.
42. Zhu J. T helper 2 (Th2) cell differentiation, type 2 innate lymphoid cell (ILC2) development and regulation of interleukin-4 (IL-4) and IL-13 production. *Cytokine*. 2015;75(1):14–24.
43. Wichner K, Stauss D, Kampfrath B, et al. Dysregulated development of IL-17- and IL-21-expressing follicular helper T cells and increased germinal center formation in the absence of RORγt. *FASEB J*. 2016;30(2):761–774.
44. Quinn JL, Axtell RC. Emerging role of follicular T helper cells in multiple sclerosis and experimental autoimmune encephalomyelitis. *Int J Mol Sci*. 2018;19(10):3233.
45. Liang D, Zuo A, Shao H, et al. Retinoic acid inhibits CD25+ dendritic cell expansion and $\gamma\delta$ T-cell activation in experimental autoimmune uveitis. *Invest Ophthalmol Vis Sci*. 2013;54(5):3493–3503.
46. Ohara D, Takeuchi Y, Hirota K. Type 17 immunity: novel insights into intestinal homeostasis and autoimmune pathogenesis driven by gut-primed T cells. *Cell Mol Immunol*. 2024;21(11):1183–1200.
47. Jie XL, Luo ZR, Yu J, et al. Pi-Pa-Run-Fei-Tang alleviates lung injury by modulating IL-6/JAK2/STAT3/IL-17 and PI3K/AKT/NF-κB signaling pathway and balancing Th17 and Treg in murine model of OVA-induced asthma. *J Ethnopharmacol*. 2023;317:116719.
48. Said A, Bock S, Lajqi T, Müller G, Weindl G. Chloroquine promotes IL-17 production by CD4+ T cells via p38-dependent IL-23 release by monocyte-derived Langerhans-like cells. *J Immunol*. 2014;193(12):6135–6143.
49. Chang Y, Bach L, Hasiuk M, et al. TGF-β specifies TFH versus TH17 cell fates in murine CD4+ T cells through c-Maf. *Sci Immunol*. 2024;9(93):eadd4818.
50. Zhong C, Liu F, Hajnik RJ, et al. Type I interferon promotes humoral immunity in viral vector vaccination. *J Virol*. 2021;95(22):e0092521.
51. Lin W, Szabo C, Liu T, Tao H, Wu X, Wu J. STING trafficking activates MAPK-CREB signaling to trigger regulatory T cell differentiation. *Proc Natl Acad Sci USA*. 2024;121(29):e2320709121.

Investigative Ophthalmology & Visual Science